Thermal and second-law analysis of a micro- or nanocavity using direct-simulation Monte Carlo

Alireza Mohammadzadeh, Ehsan Roohi, Hamid Niazmand, Stefan Stefanov, and Rho Shin Myong

Thermal and Second-Law Analysis of A Micro- or Nano-Cavity Using Direct-Simulation Monte Carlo

Alireza Mohammadzadeh   **Ehsan Roohi**

Hamid Niazmand

Department of Mechanical Engineering, Faculty of Engineering,
Ferdowsi University of Mashhad, PO Box: 91775-1111, Mashhad, Iran.

Stefan Stefanov[1]

Institute of Mechanics, Bulgarian Academy of Science,
Acad. G. Bontchev str., 1113, Sofia, Bulgaria.

Rho Shin Myong

Department of Aerospace and System Engineering, Research Center for Aircraft Parts
Technology, Gyeongsang National University, Jinju, Gyeongnam 660-701, South Korea.

ABSTRACT

In this study direct simulation Monte Carlo (DSMC) method is utilized to investigate thermal characteristics of micro- or nano-cavity flow. The rarefied cavity flow shows unconventional behaviours which cannot be predicted by the Fourier law, the constitutive relation for the continuum heat transfer. Our analysis in this study confirms some recent observations and shows that the gaseous flow near the top-left corner of the cavity is in a strong non-equilibrium state even within the early slip regime, Kn=0.005. As we obtained slip velocity and temperature jump on the driven lid of the cavity, we reported meaningful discrepancies between the direct and macroscopic sampling of rarefied flow properties in the DSMC method due to existence of non-equilibrium effects in the corners of cavity. The existence of unconventional non-equilibrium

---

[1]corresponding author

heat transfer mechanisms in the middle of slip regime, Kn=0.05, results in appearance of cold-to-hot heat transfer in the micro-cavity. In the current study we demonstrate that existence of such unconventional heat transfer is strongly dependent on the Reynolds number and it vanishes in the large values of the lid velocity. As we compared DSMC solution with the results of regularized 13 moments (R13) equations, we showed that the thermal characteristic of the micro-cavity obtained by the R13 method coincides with the DSMC prediction. Our investigation also includes the analysis of molecular entropy in the micro-cavity to explain the heat transfer mechanism with the aid of the second law of thermodynamics. To this aim, we obtained the two dimensional velocity distribution functions to report the molecular-based entropy distribution, and show that the cold-to-hot heat transfer in the cavity is well in accordance with the second law of thermodynamics and takes place in the direction of increasing entropy. At the end we introduce the entropy density for the rarefied flow and show that it can accurately illustrate departure from the equilibrium state.

I. INTRODUCTION

Micro- or nano-electro-mechanical systems (MEMS/NEMS) are widely utilized in many practical applications including mechanical engineering and biomedical devices. The study of gaseous flow in micro and nano scales has been an interesting and appealing topic of researches in recent years. It is well known that the traditional Navier-Stokes (NS) equations fail to predict

the flow features as characteristic length enters micro range and beyond. Knudsen number, which is defined as the ratio of the mean free path in the gas to the characteristic length of the flow domain, $Kn=\lambda/L$, is a measure to determine degrees of gas rarefaction. A well-established classification of the gaseous flow regimes exists in microfluidics according to the Knudsen number range [1, 2]. According to this classification, the state of a gaseous flow can be defined in four different regimes. Gaseous flow at $Kn<0.001$ is termed as continuum regime where the basic NS equations with no-slip/jump boundary conditions are valid in this regime. Gaseous flow with Knudsen number ranges of $0.001<Kn<0.1$ is called slip flow. Special treatments such as applying velocity slip and temperature jump boundary conditions on the walls should be considered in the NS equations to capture slightly rarefied flow features in the slip regime. Transition regime is termed for gas flows within $0.1<Kn<10$. In this regime, the NS equations lose validity and the well-known first order shear stress and heat flux approximations fail to predict flow behaviour. Flow is considered as free molecular if $Kn>10$. However, this classification is based mostly on data obtained from experiments and numerical studies of isothermal gaseous flows in long microchannels having simple 1-D geometries. For gaseous flows in 2D and 3D bounded domains with more complex geometries, the range of slip flow regime as defined above is questionable and should be reconsidered for each studied problem separately.

Different velocity slip models of varying complexity have been suggested to capture non-equilibrium effects in the slip regime [3-5]. Extending the Lattice Boltzmann equations to the rarefaction regimes has been another appealing approach in modelling non-equilibrium phenomena [6-11]. In addition, high-order moment methods such as R13 and R26 are alternative powerful approaches in capturing non-equilibrium phenomena [12, 13]. For example, it is

reported that the predicted results of R13 and R26 methods for rarefied Couette and Poiseuille flows are accurate in early and mid-transition regimes, respectively [13]. Despite the considerable efforts to derive higher order equations, discrete molecular modeling of direct simulation Monte Carlo (DSMC) remains a basic tool to model flow field in all degrees of rarefaction [14].

The driven cavity flow is a model problem with simple 2D geometry that can be related to many industrial applications [15]. Previously the vortex gas flow in a lid driven cavity has been studied for different regimes by several authors [16-20]. Recently the attention of some researchers has been turned to non-classical thermal behaviors of lid-driven cavity flow. Struchtrup et al. [21] used regularized 13 moments equation to show that R13 equations are capable of capturing non-equilibrium thermal phenomena in the early transition regime inside a micro-cavity. John et al. [22] utilized the DSMC technique in the micro lid-driven cavity in the transition and free molecular regimes to show the cold-to-hot heat transfer. They attributed their observations to the non-equilibrium effects inside the flow field. John et al. [23] also studied the effect of incomplete surface accommodation on the heat transfer in the lid driven cavity. They reported that decreasing the thermal surface accommodation changes the isothermal wall cavity into the adiabatic wall cavity, and reduces the strength of sudden expansion in the driven cavity.

In the present study, we have focused on the slip regime to meaningfully compare and physically interpret the discrepancies between the DSMC and NS thermal solutions. At first it is aimed to describe the physical reasons for appearance of unconventional cold-to-hot heat flux, and then we use the DSMC solution to find the responsible terms for such flux of energy. In accordance with our physical reasoning, it is demonstrated that the lid velocity significantly affects the heat flux direction. In other words, in a fixed Knudsen number the cod-to-hot heat transfer changes

into the conventional Fourier heat transfer as a consequence of gradual increase in the driven lid velocity. We also present the solution of regularized 13 moments (R13) equations in the cavity flow to investigate the capability of more accurate continuum approaches in capturing non-equilibrium heat transfer phenomenon. Afterwards the process of cold-to-hot heat transfer is studied based on the second law of thermodynamics point of view. Molecular-based entropy distribution is obtained and it is illustrated that such direction for flux of energy is indeed in the direction of increasing entropy. Furthermore, the entropy density is introduced as a tool to specify degrees of rarefaction and depicted to shows the local departure from equilibrium state. According to the best knowledge of the authors, investigating the details of thermal properties of cavity flow in the slip regime and providing the physical reasoning for the unconventional behaviors in the cavity geometry, as well as providing the entropy-based explanations for the anomalous heat flux direction are not reported elsewhere and will be the focus of the current study.

II. DSMC APPROACH

The DSMC method used in this paper follows the scheme proposed by Bird [1]. DSMC is a particle method based on the kinetic theory for simulation of the dilute gases. The method is carried out by modeling the gas flow using many independent simulating particles. Each simulating particle is representative of a large number of real gas molecules in the flow field. The time step Δt in the DSMC method is chosen as small as the motion of particles and their collisions could be decoupled at each time step. In order to implement DSMC, flow field must be divided into computational cells. The size of each cell should be small enough to result in small changes in thermodynamic properties across each cell. The cells provide geometric boundaries

and volumes required for sampling the macroscopic properties. They are also used as a unit where only molecules located within the same cell at a given time are allowed for collision. The cells are then divided into subcells in each direction to facilitate the selection of collision pairs.

In the current study, the previous code of Roohi and co-workers [24-30] is extended to simulate rarefied flow in micro- or nano- cavity. The variable hard sphere (VHS) collision model is used to consider accurate variation of viscosity with temperature. Collision pairs are chosen based on the no time counter (NTC) method, in which the computational time is proportional to the number of the simulating particles [1]. Monatomic argon, $m=6.63\times10^{-26}$ Kg and $d=4.17\times10^{-10}$ m is considered as the gaseous medium. To satisfy the cell size limitation, the cell dimensions Δx, Δy are considered as $0.1\times\lambda$. 32 particles are initially set in each cell to minimize the scattering noise. By considering full thermal accommodation coefficient, $\sigma_T =1$ all walls behave as diffuse reflectors. In order to minimize the statistical scattering, molecular properties are sampled over large period of time after the flow reaches the steady state condition. These time-averaged data are then used to obtain the thermodynamic parameters such as temperature, density, and pressure. In addition, a filtering post processor is performed to minimize the scattering in the predicted results, particularly in temperature. In this filtering, the sampled macroscopic properties (F) are averaged over a pattern of five neighboring cells, as given below.

$$F'_{(N)} = \frac{F_N + \sum\limits_{I=1}^{I=N_{neighbour}} F_I}{N_{neighbour} + 1}$$

(1)

III. THE NS EQUATIONS WITH SLIP/JUMP BOUNDARY CONDITIONS

The compressible NS equations can be derived from the Chapman-Enskog expansion of the Boltzmann equation. These equations, namely conservation of mass, momentum and total energy, are expressed as [31]:

$$\frac{\partial \rho}{\partial t} + \nabla.[\rho \mathbf{V}] = 0 \tag{2}$$

$$\frac{\partial (\rho \mathbf{V})}{\partial t} + \nabla.[\mathbf{V}(\rho \mathbf{V})] + \nabla p + \nabla.\boldsymbol{\tau} = 0 \tag{3}$$

$$\frac{\partial (\rho E)}{\partial t} + \nabla.[\mathbf{V}(\rho E)] + \nabla.[\mathbf{V}p] + \nabla.(\boldsymbol{\tau}.\mathbf{V}) + \nabla.\mathbf{q} = 0 \tag{4}$$

where ρ is the mass density, p is the pressure, $E = e + |\mathbf{V}^2|/2$ is the total energy, e is the internal energy per unit mass, $\mathbf{q}$ is the diffusive flux of heat that obtains by Fourier law [31] and $\boldsymbol{\tau}$ is the shear stress tensor that obtains by Stokes law [31]. In order to consider rarefaction effects, the first-order velocity slip and temperature jump boundary conditions on the walls are applied as follows [32]:

$$\mathbf{V}_g - \mathbf{V}_w = -\frac{2-\sigma_u}{\sigma_u}\lambda \nabla_n (\mathbf{S}.\mathbf{V}) - \frac{2-\sigma_u}{\sigma_u}\frac{\lambda}{\mu}\mathbf{S}.(\mathbf{n}.\prod_{mc}) - \frac{3}{4}\frac{\mu}{\rho}\frac{\mathbf{S}.\nabla T}{T} \tag{5}$$

$$T_g - T_w = -\frac{2-\sigma_T}{\sigma_T}\frac{2\gamma}{(\gamma+1)\mathrm{Pr}}\lambda \nabla_n T \tag{6}$$

where n represents the unit normal vector to the surface, the subscripts g and w stand for gas adjacent to wall and wall, respectively. σ_u, σ_T are the tangential momentum and thermal energy accommodation coefficients and λ is the mean free path. Both accommodation coefficients have

7

been considered as unity to simulate diffuse reflector walls. Second and third terms on the right hand side of Eq. (5) consider the effects of boundary curvature and thermal creeps on the velocity slip, respectively. For more detailed description of Eqs.(5-6) please see Ref. [32].

OpenFOAM [33] is used to solve the NS equations in the micro- or nano- lid driven cavity. The OpenFOAM, Open Field Operation and Manipulation, is a programmable CFD toolkit licensed under the GNU General Public License. The OpenFOAM is a finite-volume package designed to solve systems of differential equations in arbitrary 3D geometries. We use "rhoCentralFoam" solver to simulate subsonic micro- or nano-cavity flow. RhoCentralFoam is an explicit density-based solver for simulating the viscous compressible flow of perfect gases which benefits from a Godunov like central-upwind scheme. The space discretization has a second-order accuracy based on the reconstruction of the primitive variables of pressure, velocity and temperature; and the time integration employs the first-order (forward) Euler scheme [34].

IV. RESULTS AND DISCUSSION

A. Grid and time step independency test and code validation

The micro driven cavity considered in this study is shown in Fig. 1. Four corners of the cavity is denoted by A, B, C and D. The top driven lid moves in the positive x-direction at U_{wall} =100 m/s. Cavity flow in early, middle and border of the slip regime, i.e., Kn=0.005, 0.05 and 0.1 is considered in this study. The temperature of the walls are set equal to the reference temperature, $T_w=T_0$=300 K. Figure 2-(a) shows the vertical velocity and density profiles along the horizontal and vertical centrelines of the cavity obtained by the DSMC method. In order to perform the grid independency test, three grids composed of 100×100, 200×200 and 400×400 cells are considered. In this figure density is non-dimensionalized with respect to a reference density obtained on the driven lid.

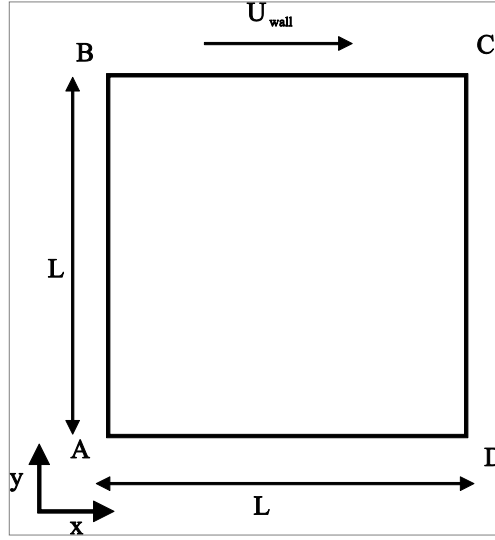**FIG. 1.** Geometrical configuration of the micro- or nano-cavity.

It is seen that the results are numerically equivalent for 200×200 and 400×400 grids; therefore, the grid containing 200×200 cells is selected for the reported results of the DSMC method in this study. For the continuum approach three grids composed of 70×70, 140×140 and 210×210 cells are chosen to investigate the mesh dependency study. Figure 2-(b) shows that the results are almost similar for 140×140 and 210×210 cells; therefore, the grid containing 140×140 cells are selected for the reported results of the continuum approach.
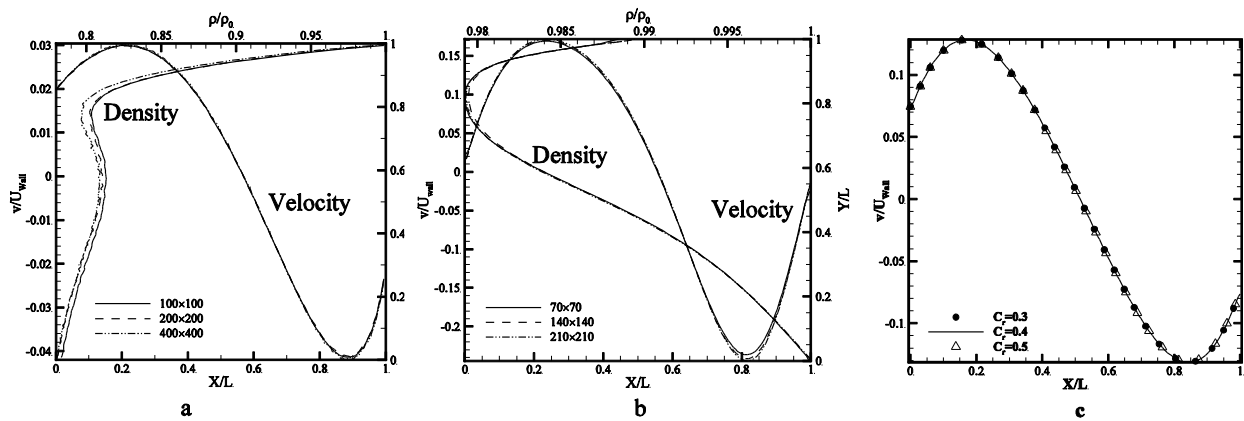

FIG. 2. Study of (a) grid independency for DSMC (b) grid independency for the NS (c) time step independency for the NS solution.

9

In order to investigate the independency of continuum results from the considered time step, we consider three Courant number, $C_r=0.3$, $C_r=0.4$ and $C_r=0.5$ and compare their results in Figure 2-(c). This figure demonstrates that the vertical component of velocity vectors along the horizontal centerlines are equivalent and the solution is independent from the chosen time step. We set $C_r=0.5$ for the rest of our NS simulations. In order to validate the NS and the DSMC results in this study, predicted pressure at Re=1.5 and Kn=0.1 is compared with the reported data of Mizzi et al. [18]. Figure 3 shows the non-dimensional pressure, p/p_0, where p_0 is the initial pressure of the rarefied flow field, for argon flow along four walls of the cavity. Small discrepancy between the two NS results is attributed to the different slip/jump boundary conditions in the NS equations. It is seen that predicted values by our DSMC solver are in good agreement with reported data of Mizzi et al. [18].
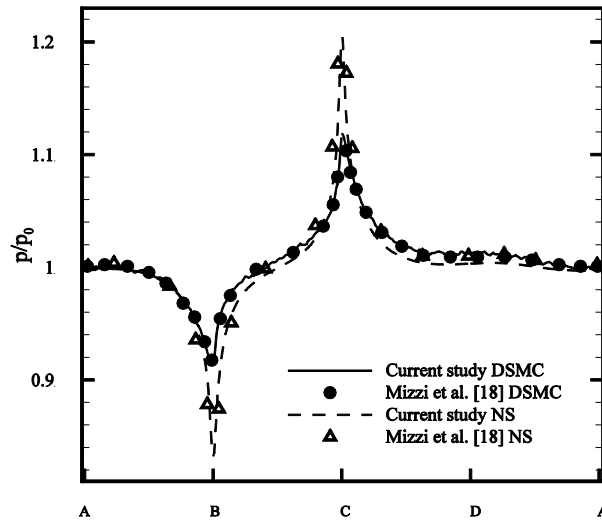
FIG. 3. Comparison of non-dimensional pressure along four walls of the cavity, Kn=0.1.

B. Comparison of the DSMC and NS solutions

1. *Slip velocity and temperature jump*

In this section, it is aimed to investigate the accuracy of NS solution in the prediction of velocity slip and temperature jump on the lid of cavity. Slip velocity and temperature jump in the DSMC

method can be obtained based on either extracting the macroscopic flow properties in the adjacent cell to the wall or direct microscopic sampling of the corresponding particle properties which strike the wall surface. For the latter, which is more consistent with definition of slip/jump phenomena, slip velocity and temperature jump are deduced from Ref. [35] as follows:

$$u_{slip} = \frac{\sum(\frac{m}{|v_p|}u_p)}{\sum(\frac{m}{|v_p|})} \tag{7}$$

$$T_{gass} - T_{wall} = \frac{1}{3R}\frac{\sum(\frac{1}{|v_p|}\|U_p\|^2) - \sum(\frac{1}{|v_p|})u_{slip}^2}{\sum(\frac{1}{|v_p|})} \tag{8}$$

where "p" indicates particle and the summation is taken over all particles striking the regarding surface. In Eq. (7), $|v_p|$ is the absolute value of normal velocity, $\|U_p\|$ is the velocity magnitude, i.e., $\|U_p\| = \sqrt{u_p^2 + v_p^2 + w_p^2}$ and R is the gas constant. Equation (7) expresses that velocity slip is literally the changes in particle velocity due to the collision with surface. Equation (8) shows that temperature jump is proportional to the changes in a fraction of total kinetic energy. Comparison of the slip velocity along the driven lid predicted by the NS and the two DSMC approaches (direct or microscopic sampling and macroscopic sampling) are shown in Fig. 4. As expected, increasing the Knudsen number results in increasing the slip velocity along the top wall. Figure 4 reveals that the discrepancy between NS and DSMC results enlarges near the top corners of the cavity, where non-equilibrium effects are dominant. Figure 4 also shows a discrepancy between macroscopic and microscopic approaches in the DSMC solution. Moreover, it is seen that the macroscopic approach, which accounts for the properties of all particles lying in the adjacent cell

11

to the surface, predicts a more continuum-like distribution of slip velocity along the driven lid of cavity. It should be noted that microscopic distribution is asymmetric. In other words, due to the direction of lid motion, slip values are slightly larger at the right corner of cavity. Additionally, in contrast to the continuum-like slip velocity, microscopic slip is finite and does not diverge at the corner.
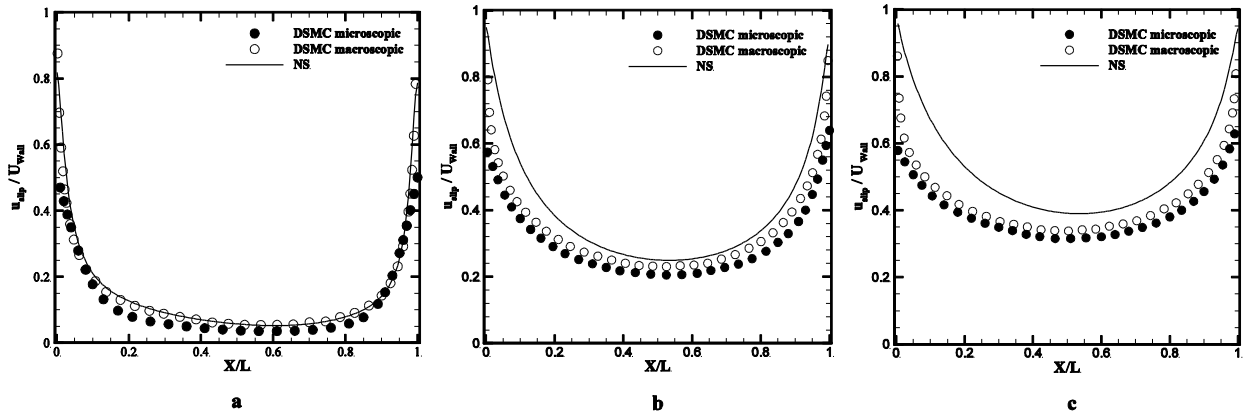
FIG. 4. Comparison of slip velocity along the driven lid from the DSMC and NS solutions at (a) Kn=0.005, (b) Kn=0.05, (c) Kn=0.1

Figure 5 shows the predicted temperature jump of the rarefied flow along the driven lid of cavity. At Kn=0.005 the employed temperature jump boundary condition shows effectiveness in predicting temperature trend far from the top corners. Although in the middle of slip regime the departure from equilibrium state is quite small, the temperature jump boundary condition shows total incapability in predicting temperature trend in Figure 5-b. According to the continuum equations, the increase in the temperature is mostly due to the viscous dissipations. As Knudsen number increases the velocity gradients in the flow field decreases, which subsequently reduces flow temperature. Figure 5 also shows that similar to the NS solution, the macroscopic approach in the DSMC method predict a decrease in the temperature near the top left corner. Comparison of the two DSMC solutions indicates that particles near the top-left corner are in non-

equilibrium state. Limited inter-molecular collision due to rapid motion of the driven lid in this region brings about significant departure from equilibrium state. This leads to a clear conclusion that the first order macroscopic slip/jump boundary conditions loose accuracy close to the corner even at a very low Kn number of 0.005. This conclusion is expected because most of slip/jump boundary conditions are derived assuming the continuity of velocity distribution function parallel to the boundary surface. Therefore, extension of these equations to more complex geometries with strong curvature or existence of singular points may be erroneous.
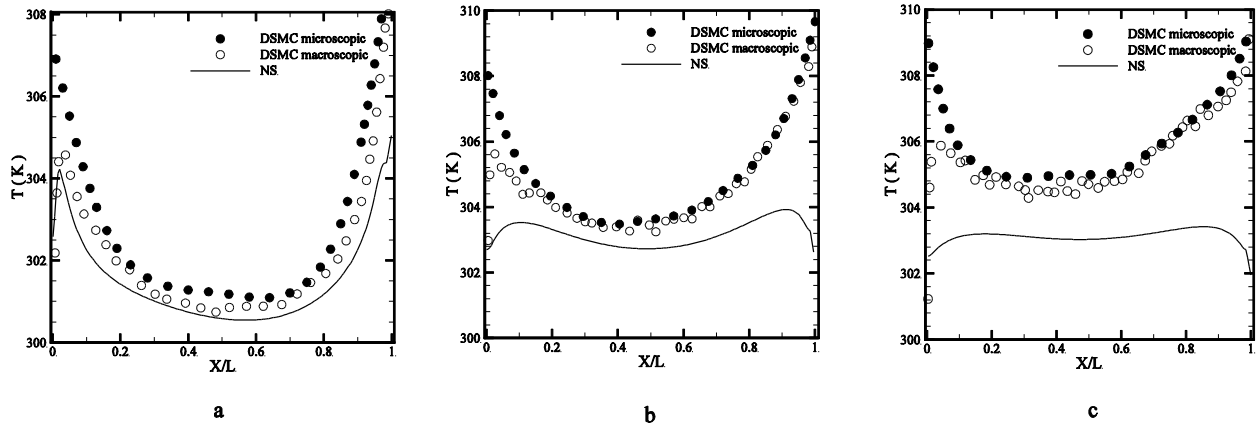

FIG. 5. Comparison of rarefied flow temperature jump along the driven lid of the cavity from the DSMC and NS solutions at (a) Kn=0.005, (b) Kn=0.05, (c) Kn=0.1

2. Heat flux behaviour

Figure 6 shows the conductive heat flux lines overlaid on the temperature contours predicted by NS and DSMC methods. In an isothermal wall cavity, the viscous dissipation is the main mechanism to change the gas temperature inside the flow field. Clearly, the viscous dissipation always acts as a heat source and is dominant where the shear stresses are strong. The shear stress values are large in proximity of the driven lid near the top right corner of cavity. Besides the viscous dissipation, significant pressure variation prevailing near the top corners of cavity affect the temperature field, see Fig. 3. In addition to all, the non-equilibrium effects which are in turn

13

dominant at the top corners of cavity influence the thermal field. The interplay between these

phenomena determines the thermal characteristic of the rarefied flow inside the cavity.
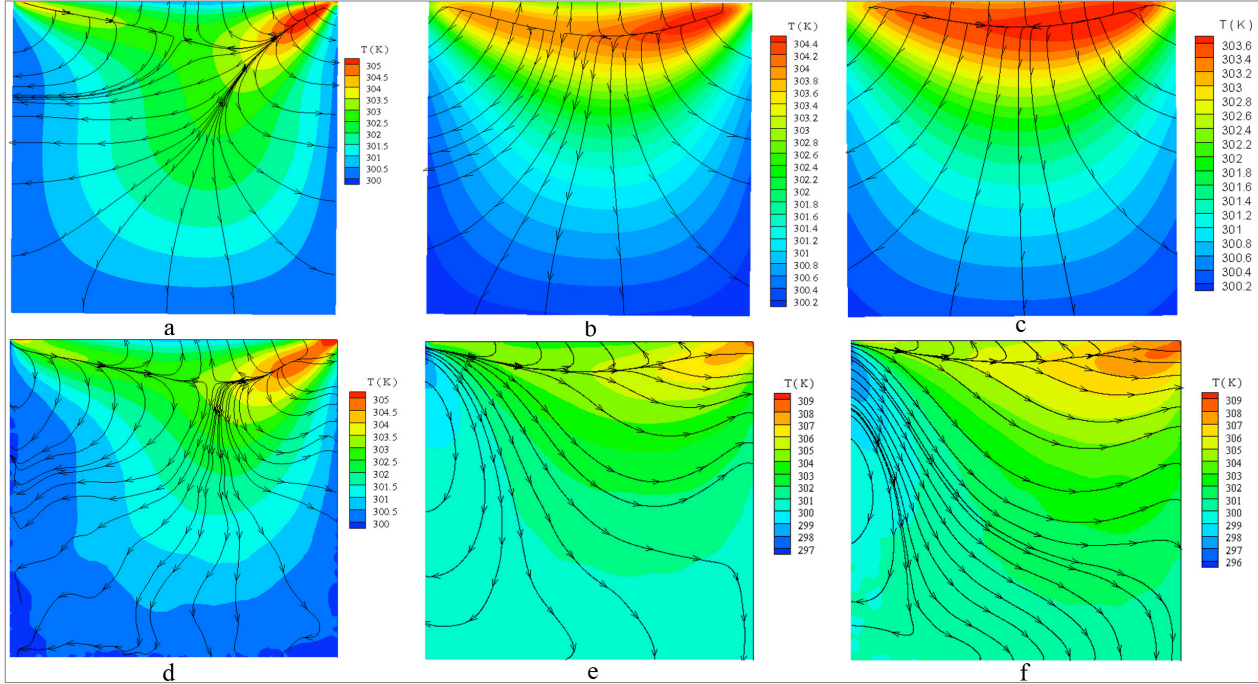
FIG. 6. (Color online) Conductive Heat flux lines overlaid on the temperature contour, top row: NS, bottom row: DSMC, (a) and (d) Kn=0.005, (b) and (e) Kn=0.05, (c) and (f) Kn=0.1

In the early slip regime, as shown in Fig. 6-(a) and Fig. 6-(d), predicted distribution of

temperature obtained by the NS equations are in approximate agreement with the molecular

approach. Both methods predict almost similar range of temperature variation in the flow field.

In addition, the shapes of temperature contours are quite similar. The predicted direction of

conductive heat flux by the DSMC is from hot to cold regions over the entire domain except for

a small area near the top right corner. Temperature distribution in the middle slip regime

obtained by the NS equations is shown in Fig. 6-(b). Maximum viscous dissipation occurs where

the largest velocity gradients exist. As a result, the proximity of the top right corner, where the

maximum shear stress occurs, is predicted as the hottest region by the NS equations. Figure 6-(e)

shows the temperature contour from the DSMC results at Kn=0.05. It is seen that the maximum temperature for the DSMC solution is greater than the predicted value by the continuum approach. Moreover, reduction in flow temperature near the left wall shows that the sudden expansion of rarefied flow in this region dominates the existing heat transfer mechanisms. Surprisingly, in the middle of slip regime, the conductive heat flux lines are from colder to the hotter regions in the upper half of the cavity. The assumed constitutive law of Fourier heat conduction, $\mathbf{q} = -k\nabla T$, incorporated in the NS equations, cannot predict such direction for transfer of heat. Conductive heat flux vector in the DSMC method is obtained by the following molecular dynamic relations:

$$q_x = \frac{1}{2}[\rho(\overline{\|\mathbf{U}_p\|^2 u_p} - \overline{\|\mathbf{U}_p\|^2}u_0) - 2p_{xx}u_0 - 2p_{xy}v_0] \qquad (9)$$

$$q_y = \frac{1}{2}[\rho(\overline{\|\mathbf{U}_p\|^2 v_p} - \overline{\|\mathbf{U}_p\|^2}v_0) - 2p_{xy}u_0 - 2p_{yy}v_0] \qquad (10)$$

where $p_{i,j} = \rho\overline{c_{p,i}'c_{p,j}'}$ is the pressure tensor, $c_{p,i}$ is the ith component of the microscopic velocity vector and $c_p'=c_p-c_0$. Figure 6-(e) reveals that in a simple two dimensional cavity flow, even in the middle slip regime, the direction of heat flux cannot be predicted by the NS equations. Figure 6-(c) shows conductive heat flux lines obtained by the NS solution at Kn=0.1. Temperature distribution is very similar to the previous case; however, the maximum temperature is decreased. Smaller shear stress at Kn=0.1 in comparison with Kn=0.05 decreases viscous dissipation, the dominant heat generation mechanism in the NS equation, which in turn reduces the maximum temperature in the flow field. Figure 6-(f) shows the conductive heat flux lines in the cavity from the DSMC solution at Kn=0.1. The conductive heat flux lines and temperature contours are quite similar to the previous test case; however, the minimum temperature is

decreased by one degree that demonstrates stronger non-equilibrium effects in the top left corner of the cavity.

The sharp corners in the cavity geometry generate a bend in the velocity profile near the top corners, and consequently the second derivative of velocity increases in this region. The interplay between temperature gradient and second derivative of velocity determines the direction of conductive heat flux in the cavity. Small variation in the flow temperature, due to relatively small lid velocity, results in domination of heat flux related to the second derivative of velocity, cold-to-hot, over the conventional Fourier heat flux. On the other hand, as Knudsen number decreases the intermolecular collision takes place more frequently, and consequently the diffusive heat flux (corresponding to the temperature gradient) overcomes the heat flux due to the second derivatives of velocity. In accordance with the current observations, weakly non-linear form of the Boltzmann equation attributes higher order heat flux terms to the second derivative of velocity, see Ref. [36].

We also investigate the conductive heat flux lines in two other conditions to describe the criteria in which the cold-to-hot heat flux remains dominant. Figures 7-(a-b) show the conductive heat flux lines obtained by DSMC method at Kn=0.05 when the lid velocity is assumed to be at U=200 m/s and U=400 m/s, respectively. It is seen that increasing the lid velocity results in reappearance of a region with hot-to-cold energy transfer near the top right corner. Comparison of Fig. 6-(e) with Fig. 7 shows that as the lid velocity increases, the flow field encounters wider range of temperature variations. Due to domination of temperature gradient over the second derivative of velocity, the region with the conventional hot-to-cold heat flux extends. Therefore, cold-to-hot heat flux phenomenon in the micro-cavity is limited to low Reynolds-low Mach number conditions.

16
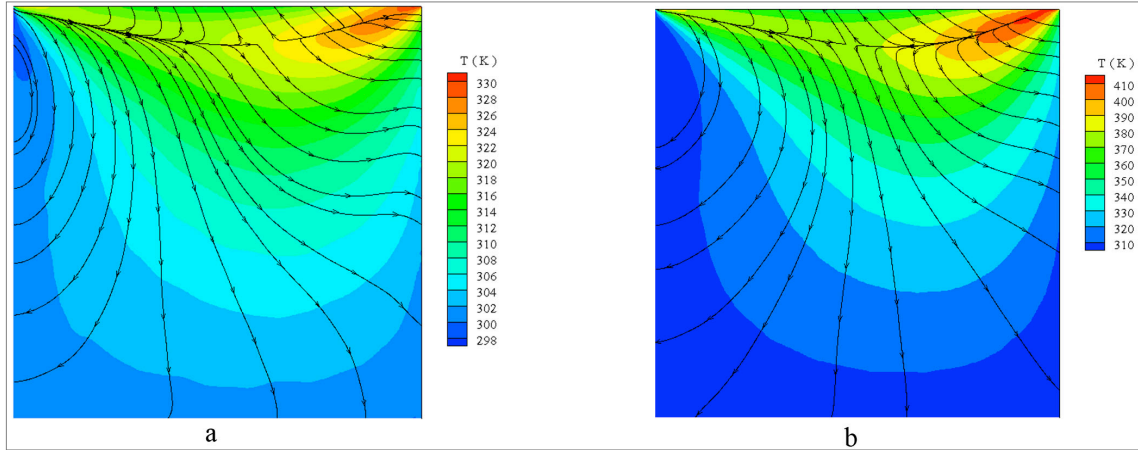
FIG. 7. (Color online) Heat flux lines overlaid on the temperature contour for (a) U_{wall}=200 m/s, (b) U_{wall}=400 m/s.

In order to provide a numerical explanation for the anomalous direction of energy via DSMC method, the components of conductive heat flux vector reported in Eqs. (9-10) at Kn=0.05 are shown in Fig. 8. The obtained heat flux lines by the first terms on the right hand side of Eqs. (9-10) are shown in Figure 8-(a). It is seen that the corresponding heat flux lines to the first terms are quite similar to the velocity streamlines in the cavity. Heat flux lines, obtained by the second terms on the right hand side of Eqs. (9-10), are shown in Figure 8-(b). These terms are basically in the opposite direction of horizontal velocity component in the entire domain. Comparison of Figure 8-(a) and 8-(b) shows that the interplay between the first and the second terms of the heat flux equations determines the heat flux direction particularly in the upper half of cavity. The effects of the third terms on the heat flux lines are shown in Figure 8-(c), which is also in the opposite direction of the vertical velocity component throughout the temperature field.
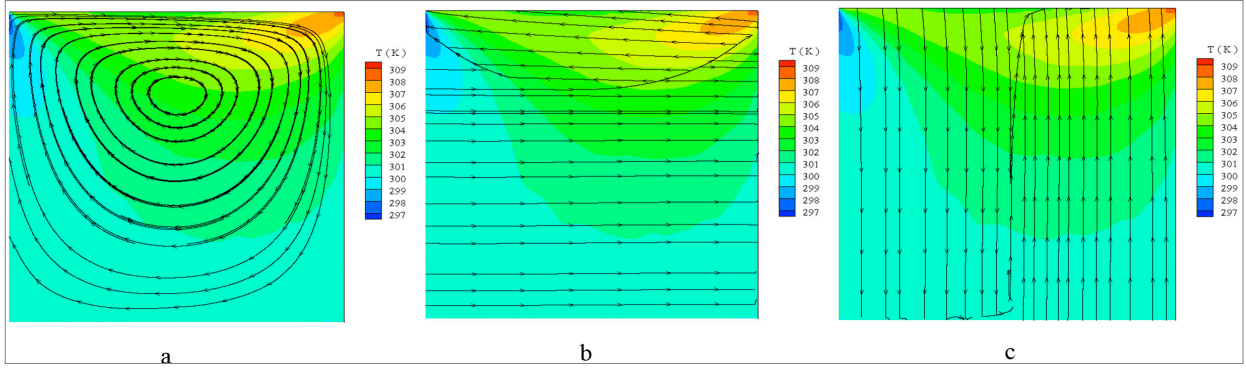
FIG. 8. (Color online) Components of heat flux vectors overlaid on the temperature contour for the DSMC solution at
Kn=0.05, (a) first term, (b) second term, (c) third term.

Clearly, the simple constitutive law of Fourier heat conduction in the NS equations fails to predict thermal characteristics of the flow even in the middle slip regime. As a result, we were intended to find the capability of the extended continuum-based methods in capturing non-equilibrium heat transfer phenomena. We present the solution of the full R13 equations for the driven cavity flow at Kn=0.05. Description of the R13 governing equations is given in Ref. [37].
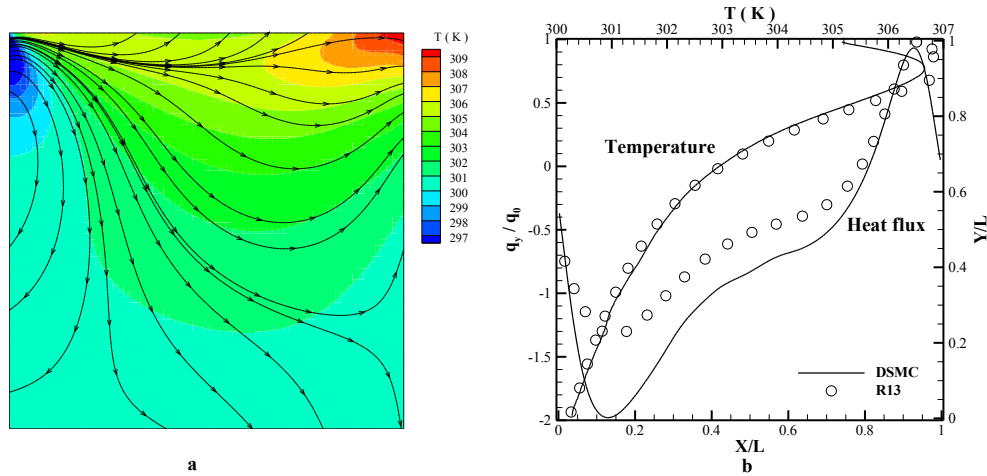
FIG. 9. (Color online) (a) Heat flux lines obtained using full R13 equations (b) comparison of vertical heat flux and temperature profile along Y/L=0.8 and X/L=0.8 line from the DSMC and R13 solutions.

Figure 9-(a) shows the conductive heat flux lines overlaid on the temperature distribution predicted by the R13 method. It is seen that the full R13 equations can capture cold-to-hot heat flux phenomenon in the middle of slip regime. This figure also illustrates that the predicted temperature distribution by the regularized 13 moment method are similar to the DSMC solution in Fig. 6. Figure 9-(b) shows the comparison of non-dimensional vertical heat flux and temperature profile along Y/L=0.8 and X/L=0.8, respectively. In this figure, heat flux is non-dimensionalized by its maximum positive value along the horizontal line. It is well observed that the predicted temperature by the R13 methods is in good agreement with the DSMC solution. Although the heat flux profile exhibits a small error in the magnitude, the heat flux direction is correctly predicted. It is expected that employing higher moment methods, i.e., R26, provide closer agreement with DSMC solution [13].

3. Entropy distribution

In this section it is aimed to focus on the entropy distribution in the flow field. Entropy can provide useful information about the direction of existing processes in the cavity such as conductive heat flux. It is well known that each process develops in the direction of increasing entropy [38]. According to the molecular gas dynamics theory, the transport equation for the entropy is expressed by [39]:

$$\frac{\partial}{\partial t} S(\mathbf{r}, t) = -\nabla \cdot [\mathbf{J_s}(\mathbf{r}, t) + S\mathbf{V}] + \sigma_{ent}(\mathbf{r}, t)$$

(11)

where S represents the local entropy, $\mathbf{J_s}$ is the flux of entropy by the molecular velocities and σ_{ent} shows the production of entropy in the flow field. The molecular velocity distribution functions are utilized to obtain entropy in the molecular gas dynamics. In fact, the local departure

from the equilibrium Maxwellian distribution function, determines the variation of entropy in the flow field. According to the molecular gas dynamics theory, entropy is expressed as [40]:

$$S = k_{Boltz} \sum_{bins} F_{bin}(c)(1 - \ln(F_{bin}(c))\Delta c \qquad (12)$$

where k_{Boltz} is the Boltzmann constant, Δc is the width of velocity bin and $F_{bin}(c)$ is the local three dimensional velocity distribution function. Since obtaining the three dimensional velocity distribution function is numerically expensive, and sometimes impossible, we divided the $F(c)$ function to a planer, $f_{x,y}$ and a one dimensional normal to the flow field distribution function, f_z. It is worth noting that such assumption is permitted as long as the particles encounter Maxwellian distributed function normal to the micro-cavity.

$$F(c) = f_{x,y} \cdot f_z \qquad (13)$$

Figure 10 shows the velocity distribution function in the top left corner of the cavity. As was expected, the f_z is very similar to the equilibrium Maxwellian distribution, which confirms the validity of our assumption. By considering the specified velocity distribution functions, the molecular entropy is then expressed as:

$$S = k_{Boltz} \sum_{bin}[1 - f_{x,y} \cdot f_z \ln(f_{x,y} \cdot f_z)\Delta c_{x,y}\Delta c_z] \qquad (14)$$
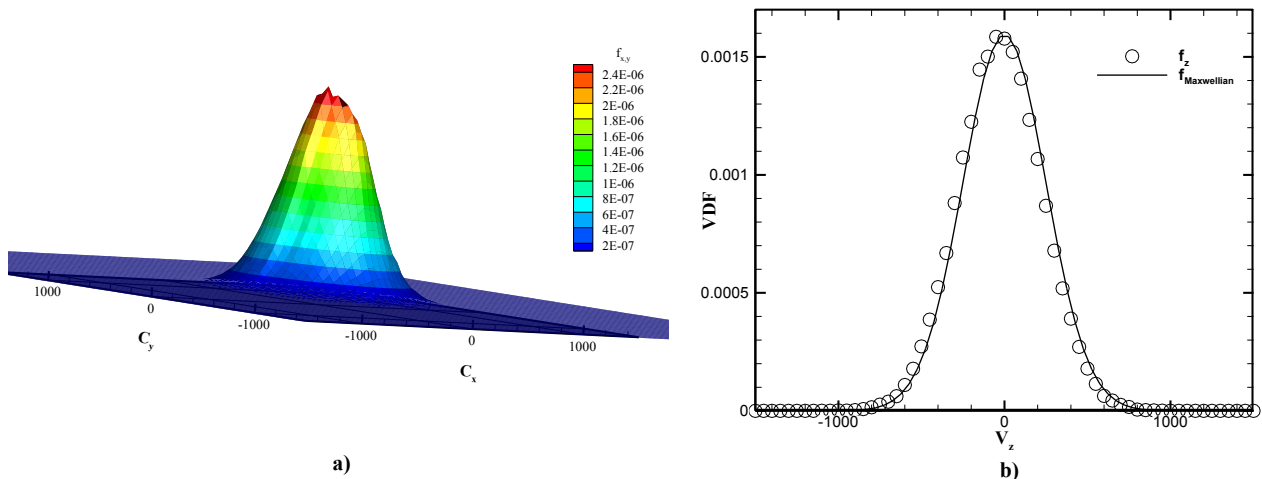
a)

b)

20

a) $f_{x,y}$, b) f_z

Figure 11 shows the entropy distribution obtained by the DSMC method. This figure demonstrates that, in all degrees of rarefaction, entropy increases in the direction of flow. Moreover, as non-equilibrium effect enlarges, the rarefied flow encounters wider range of entropy variation. In other words, more pronounced departure from the equilibrium velocity distribution function, brings about higher level of entropy in the rarefied flow. This figure also illustrates that the shape of entropy distribution in the cavity is similar to the temperature contour, see Fig. 6. Temperature in the molecular dynamic theory is the variance of molecular velocity. The variance of this value shows the disorder in the molecular velocity and the departure from the equilibrium distribution which coincides with the very definition of entropy. In accordance with the second law of thermodynamics, Fig. 11 also shows that the conductive heat flux lines are in the direction of increasing entropy in the flow field. Although cold-to-hot heat transfer in the cavity seems unconventional, it is totally in the direction of increasing entropy in the flow field.
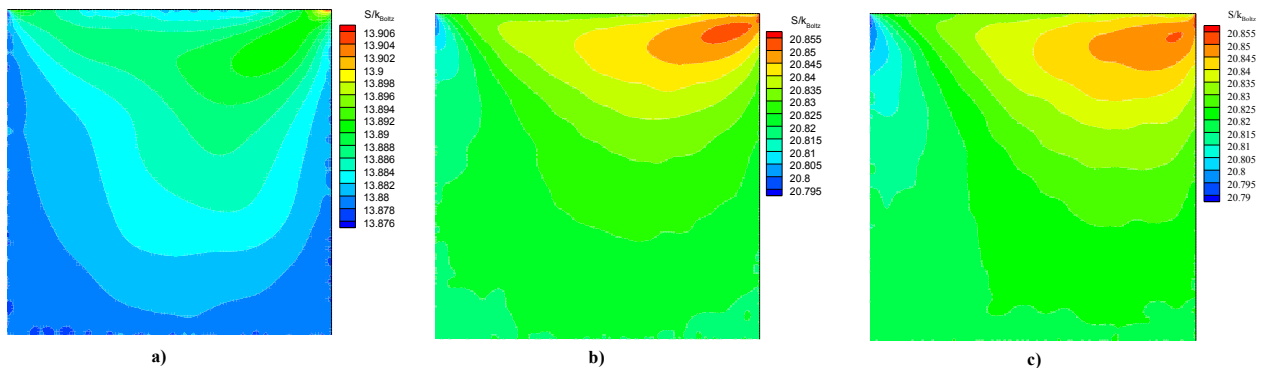
FIG. 11. (Color online) Distribution of entropy in the cavity predicted by the DSMC at
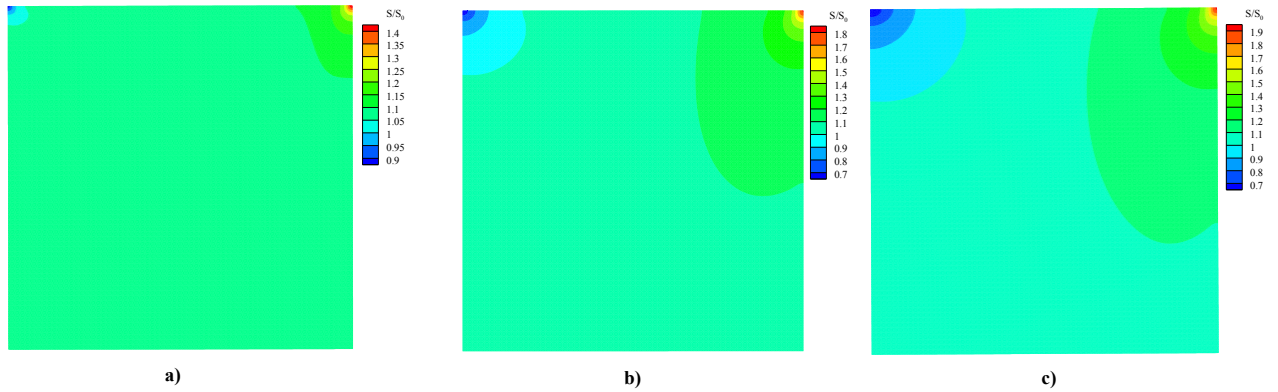(a) Kn=0.005, (b) Kn=0.05, (c) Kn=0.1

In the current study we also used the continuum approach to investigate the entropy distribution in the micro-cavity. The transport equation of the entropy in the continuum approach is expressed as [39]:

$$\frac{\partial}{\partial t}S(\mathbf{r},t) = -\nabla.[\frac{\mathbf{q}}{T}+S\mathbf{V}]+\sigma_{ent}(\mathbf{r},t) \tag{15}$$

Where $\mathbf{q}$ represents the Fourier heat flux in the flow field. Comparing Eq. 11 with Eq. 15 reveals that in the continuum approach, $\frac{\mathbf{q}}{T}$ replaces the flux of entropy by means of molecular velocities in the DSMC method. The entropy defined for the reversible processes in the macroscopic approach can be obtained based on the local pressure and density, and is expressed as [41]:

$$S = \rho s = \rho\ln(\frac{P}{\rho^{\gamma}}) \tag{16}$$

where γ is the gas specific heat ratio. Figure 12 shows the entropy distribution obtained by continuum approach in the Knudsen regimes. In this figure the entropy is non-dimensionalized with respect to the initial entropy, S_0 in the flow field. This figure illustrates that similar to the molecular method, the continuum approach predicts that maximum entropy is located near the top right corner of the cavity. In addition, increasing the Knudsen number leads to a wider range of entropy variation in the flow field.

FIG. 12. (Color online) Distribution of entropy in the cavity predicted by the continuum approach at

At this stage it is aimed to obtain the entropy flux, $\boldsymbol{J}$ in the DSMC method. Entropy flux is the transfer of entropy via motion of molecules. Entropy flux in the molecular gas dynamics theory is obtained by [40]:

$$J = k_{Boltz} \sum_{bin} c_{bin} F_{bin}(\boldsymbol{c})[1 - \ln(F_{bin}(\boldsymbol{c}))]\Delta c \tag{17}$$

Considering the velocity distribution functions in Eq. 13, the entropy flux is then expressed as:

$$J_x = k_{Boltz} \sum_{bin} [c_x f_{x,y} \Delta c_{x,y} - c_x f_{x,y}.\ln(f_{x,y})\Delta c_{x,y} - c_x f_{x,y}.f_z.\ln(f_z)\Delta c_{x,y}.\Delta c_z] \tag{18}$$

$$J_y = k_{Boltz} \sum_{bin} [c_y f_{x,y} \Delta c_{x,y} - c_y f_{x,y}.\ln(f_{x,y})\Delta c_{x,y} - c_y f_{x,y}.f_z.\ln(f_z)\Delta c_{x,y}.\Delta c_z] \tag{19}$$
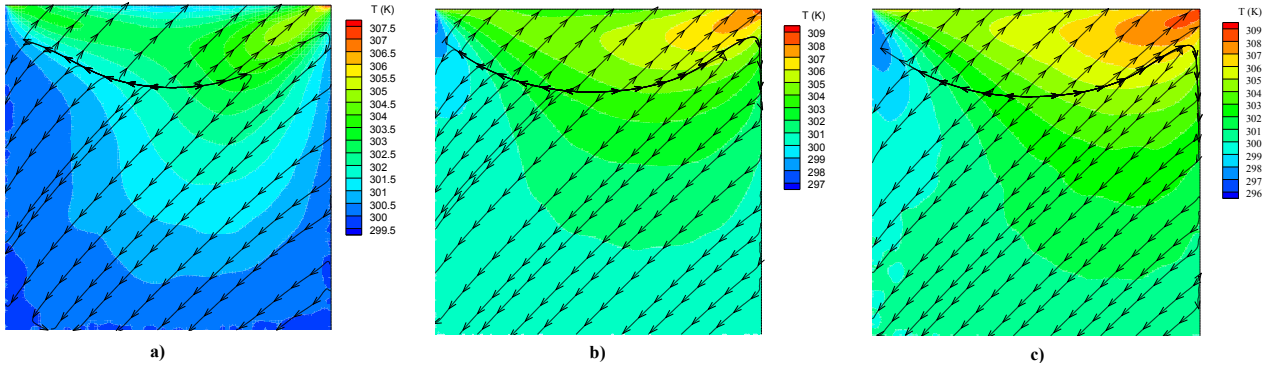
FIG. 13. (Color online) Entropy flux overlaid on the temperature distribution obtained by the DSMC method at
(b) Kn=0.005, (b) Kn=0.05, (c) Kn=0.1

Figure 13 shows the entropy flux in the micro-cavity obtained by the DSMC method. The entropy flux can provide some information about the direction of heat in the cavity as well. Comparison of Eq. 15 and 11 shows that in the equilibrium thermodynamics, the entropy flux is in the direction of conductive heat transfer. In the non-equilibrium thermodynamics theory, the entropy flux can be obtained by [40]:

23

$$J = \frac{\mathbf{q}}{T} + T^{-1}\sum x_k \psi_k \qquad (20)$$

where x_k is the generalized potentials conjugate to the non-conserved variables denoted by ψ_k. This equation reveals that, only, in the absence of non-equilibrium effects the entropy flux vector is in the direction of heat flux vector. Existence of non-equilibrium effects, particularly near the top walls of micro-cavity, leads to appearance of different direction for entropy flux and heat flux vectors.

It is now aimed to introduce the entropy density, $s = \dfrac{S}{\rho.k_{Boltz}}$ as a tool to determine the non-equilibrium effects. Figure 14 shows the distribution of entropy density in the flow field obtained from the DSMC method. It is seen that in the entire slip regime the maximum entropy density occurs near the top-left corner of the cavity. Although the rarefied flow encounters the maximum entropy in the top right corner, the entropy density is maximized near the top left corner. Backing to Fig. 5-(a), this is the same location in which the rarefied flow experience the maximum non-equilibrium (rarefaction) state.This figure demonstrates that the entropy density, and not the entropy, should be utilized to determine the departure from equilibrium state. As the entropy value is divided by the flow density, it can meaningfully show the local departure from the equilibrium for each molecule in the flow field. In other words, the entropy density, which shows the departure from the equilibrium distribution for each molecule, can determine the local degrees of rarefaction in the flow field.
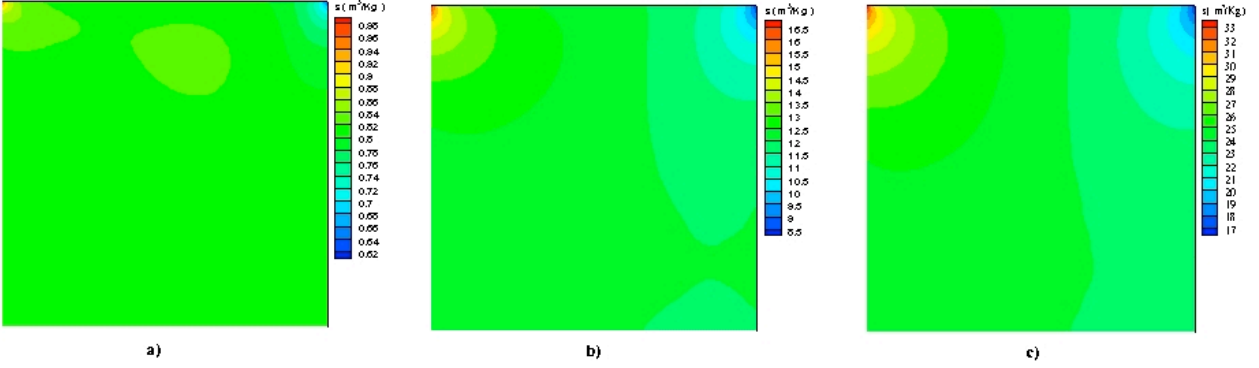
FIG. 14. (Color online) Distribution of the entropy density obtained by the DSMC method at (c) Kn=0.005, (b) Kn=0.05, (c) Kn=0.1

V. CONCLUSION

In the current study we utilized DSMC technique in a micro- or nano- lid-driven cavity in the slip regime to show that the well accepted extension of the NS equations accompanied with the slip/jump boundary conditions is not promising, and conventional border of slip regime, Kn<0.1 is not accurate for the cavity flow. We observed and confirmed the unconventional cold-to-hot heat transfer, and attributed such phenomena to the sharp bends in the velocity profiles which take place near the top corners of cavity. The small variation of the flow temperature in the cavity, due to the relatively small lid velocity, results in dominance of cold-to-hot heat transfer, i.e., heat transfer corresponding to the second derivative of velocity field, over the conventional Fourier heat flux. Our simulation indicates that increasing the wall velocity increases the temperature variations in the flow field, and subsequently results in reappearance of hot-to-cold heat transfer. We obtained velocity distribution functions and investigated the molecular-based entropy in the rarefied cavity flow. Our findings demonstrates that such unconventional direction for the heat flux is in accordance with the second law of thermodynamics, and takes place from lower to higher entropy in the micro-cavity. In addition, we obtained the entropy flux vector and show that existence of non-equilibrium effects in the micro-cavity leads to appearance of

25

different direction for entropy flux and heat flux vectors. We introduced the entropy density as a tool to determine non-equilibrium effects, and detected the top-left corner of cavity as the location of highest non-equilibrium state, where the maximum entropy density occurs.

ACKNOWLEDGMENT

REFERENCES

[1]   G. A. Bird, *Molecular gas dynamics and the direct simulation of gas flows* (Oxford university press, Oxford, 1994).

[2]   M. Gad-el-Hak, Journal of fluid engineering **121**, 5 (1999).

[3]   C. Cercignani, *The Boltzmann equation and its applications (applied mathematical sciences)* (Springer, New York, 1987).

[4]   F. Sharipov, and V. Seleznev, Journal of physical and chemical reference data **27**, 657 (1998).

[5]   N. G. Hadjiconstantinou, Physics of fluids **15**, 2352 (2003).

[6]   Y. Zhang, R. Qin, and D. R. Emerson, Physical review E **71**, 047702 (2005).

[7]   Y.-H. Zhang *et al.*, Physical review E **74**, 046704 (2006).

[8]   G.-H. Tang, Y.-H. Zhang, and D. R. Emerson, Physical review E **77**, 046701 (2008).

[9]   S. H. Kim, H. Pitsch, and I. D. Boyd, Physical review E **79**, 016702 (2009).

[10]   G. H. Tang *et al.*, Physical review E **79**, 027701 (2009).

[11]   X.-J. Gu, D. R. Emerson, and G.-H. Tang, Physical review E **81**, 016313 (2010).

[12]   H. Struchtrup, and M. Torrilhon, Physical review E **78**, 046301 (2008).

[13]   X.-J. Gu, and D. R. Emerson, Journal of fluid mechanics **636**, 177 (2009).

[14]   G. A. Bird, Physics of fluids **6**, 1518 (1963).

[15]   H. F. Oztop, and I. Dagtekin, International journal of heat and mass transfer **47**, 1761 (2004).

[16]   S. Naris, and D. Valougeorgis, Physics of fluids **17**, 097106 (2005).

[17]   D. Auld, and Y. L. Lan, in 24th applied aerodynamics conference (AIAA-3328, California, 2006).

[18]   S. Mizzi, D. R. Emerson, and S. K. Stefanov, Journal of computational and theoretical nanoscience **4**, 817 (2007).

[19]   D. A. Perumal *et al.*, International journal of recent trends in engineering **1**, 15 (2009).

[20]   D. A. Perumal, V. S. Kumar, and A. K. Dass, CFD letters **2**, 75 (2010).

[21]   H. Struchtrup, P. Taheri, and A. Rana, in 27th international symposium on rarefied gas dynamics2011).

[22]   B. John, X. J. Gu, and D. R. Emerson, Numerical heat transfer **58**, 287 (2010).

[23]   B. John, X. J. Gu, and D. R. Emerson, Computers & fluids **45**, 197 (2011).

[24]   E. Roohi, and M. Darbandi, Physics of fluids **21**, 082001 (2009).

[25]   E. Roohi, M. Darbandi, and V. Mirjalili, Journal of heat transfer **131**, 092402 (2009).

[26]   M. Darbandi, and E. Roohi, Microfluidics and nanofluidics **10**, 321 (2011).

[27]   M. Darbandi, and E. Roohi, International communication in heat and mass transfer **38**, 5 (2011).

[28]   H. Akhlaghi, E. Roohi, and S. Stefanov, International journal of thermal science (2012), In Press, DOI: 10.1016/j.ijthermalsci.2012.04.002.

[29]   O. Ejtehadi, E. Roohi, and J. Abolfazli, International communication in heat and mass transfer **39**, 439 (2012).

[30]   E. Roohi, and M. Darbandi, Applied mathematical modelling **36**, 2314 (2012).

[31]   J. D. Anderson, *Hypersonic and high temperature gas dynamics* (AIAA Press, 2007).

[32]   C. J. Greenshields *et al.*, International journal for numerical methods in fluids **63**, 1 (2009).

[33]   OpenFOAM, *The open source CFD toolbox* (user guide, version 1.6, 2009).

[34]   L. O'Hare *et al.*, International journal of heat and fluid flow **28**, 37 (2007).

[35]   A. J. Lofthouse, (University of Michigan, 2008).

[36]   Y. Sone, *Molecular gas dynamics theory, techniques, and applications* (Brikhauser, Boston, 2007).

[37]   H. Struchtrup, *Macroscopic transport equations for rarefied gas flows* (Springer, Berlin, 2005).

[38]   A. Bejan, *Entropy generation minimization: the method of thermodynamic optimization of finite-size systems and finite-time processes* (CRC Press, 1996).

[39]   B. C. Eu, *Nonequilibrium statistical mechanics: ensemble method* (Kluwer academic publishers, Dordrecht, 1998).

[40]   B. C. Eu, *Kinetic Theory and Irreversible Thermodynamics* (Wiley, New York, 1992).

[41]   K. G. Powell *et al.*, Journal of computational physics **154**, 284 (1999).